Journal of Nanofluids
Vol. 11, pp. 988–995, 2022
(www.aspbs.com/jon)

ARTICLE

Unsteady Radiative Flow of Particular Nanoliquids Along an Infinite Vertical Flat Plate in the Proximity of Convective Boundary Condition

M. Venkateswarlu[1,*], P. Rami Reddy[2], and Ali J. Chamkha[3]

[1]*Department of Mathematics, V. R. Siddhartha Engineering College, Krishna 520007, A. P, India*
[2]*Department of Mathematics, Krishna University, Krishna 521001, A. P, India*
[3]*Faculty of Engineering, Kuwait College of Science and Technology, Doha District, 35004, Kuwait*

In this article, the heat transfer and flow pattern characteristics are restudied in the proximity of convective boundary condition for three kinds of nanoliquids, namely copper oxide-water nanoliquid ($CuO–H_2O$), silver-water nanoliquid ($Ag–H_2O$), and titanium dioxide-water nanoliquid ($TiO_2–H_2O$). The thermal radiation impact is assumed into account. The partial differential equations are shifted into ordinary differential equations by applying an acceptable transformation and then exact solutions are acquired by promoting the Laplace transform technique. Solid volume fraction is fluctuated as 5%, 10%, 15%, and 20%. The variations of nanoliquid motion and energy transmit are displayed graphically as well as the numerical values of friction factor and rate of heat transfer at the plate are displayed in tabular pattern. In particular, the least shear stress occurs for silver-water nanoliquid and the greatest shear stress occurs for titanium dioxide-water nanoliquid as well as the least heat transfer coefficient occurs for titanium dioxide-water nanoliquid and the greatest heat transfer coefficient occurs for copper oxide-water nanoliquid. This report can be further utilized to authenticate the effectiveness of acquired mathematical results for another sophisticated nanoliquid stream problems.

KEYWORDS: Vertical Flat Plate, Nanoliquids, Analytical Solution, Skin Friction, Rate of Heat Transfer.

1. INTRODUCTION

Low thermal conductivity of energy transfer liquids such as water, oil, and ethylene glycol mixture is a primary limitation in enhancing the performance and the compactness of several electronic devices. To overcome this drawback, there is a strong motivation to develop advanced energy transfer liquids with substantially higher conductivities to enhance thermal properties. As such an imaginative way in upgrading thermal conductivities of a liquid is to suspend metallic nanoparticles within it. The resulting mixture referred to as a nanoliquid possesses a substantially desirable thermal conductivity compared to that of the traditional liquids. Parvin and Chamkha[1] presented the heat transfer, entropy generation, and Bejan number effects at various Rayleigh numbers and solid volume fractions in the geometry which is a combination of the horizontal and vertical enclosure shapes with water based copper nanoliquid. Kameswaran et al.[2] discussed the steady nanoliquid flow over a vertical wavy facade in the proximity of thermal stratification and convective boundary condition. Shasikumar et al.[3] presented the effects of aluminum and titanium alloy nanoparticles on viscous dissipation and joule heating in a micro-channel in the proximity convective boundary condition. Veera Krishna and Chamkha[4] informed that the radiation absorption parameter leads to escalate the thermal boundary layer thickness in the proximity of water based-silver nanoliquid as well as water based-titanium dioxide nanoliquid. Venkateswarlu et al.[5] informed that the micro-channel slip velocity and skin friction coefficient escalates with an enhancement in the Knudsen number for both symmetric and asymmetric heating cases. Dogonchi et al.[6] discussed the shape factor of nanoparticles and magnetic field by applying the volume based finite element method. Ghalambaz et al.[7] discussed the ratio between the thermal conductivity of the hybrid nanoliquid and thermal conductivity of the plate. Venkateswarlu and Bhaskar[8] concluded that the liquid heat transfer as well as Bejan number declines with an enhancement in the permeability parameter. Selimefendigil et al.[9] observed that Nusselt number escalates for grown values of solid volume fraction or Hartmann number. Chamkha et al.[10] informed that escalating the nanoparticle volume fraction has a progressive impact on the generation of

*Author to whom correspondence should be addressed.
Email: mvsr2010@gmail.com
Received: 23 February 2022
Accepted: 27 March 2022

entropy than the enhancement in the heat transfer rate. Venkateswarlu et al.[11] informed that the liquid temperature escalates with an enhancement in the Prandtl number as well as heat absorption parameter. More discussions carried out on the nanoliquid flows can be found in the Refs. [12–16].

The thermal radiation applications in our engineering and industrial domains are immense. So that, the operations are executed at an ultimate comfortably heat transfer under various non-isothermal constraints and in such circumstance where the convective heat transfer coefficients are smaller. The Rosseland approximation is applied to describe the radiative heat flux in the heat convective analysis. The radiative heat transfer is practically applicable in nuclear power plants, hypersonic flights, space vehicles, nuclear reactors, gas turbines, the model of pertinent equipment, etc. Chamkha et al.[17] observed that the boundary friction declined with escalating values of the Prandtl number, inclination angle, and magnetic parameter. Venkateswarlu et al.[18] identified that the liquid motion escalates at the cold plate and declines at the hot plate with an enhancement in the radiation parameter. Sreedevi et al.[19] presented the double diffusive hydromagnetic natural convective stream past a stretching sheet in the proximity of thermal radiation and Hall current. Venkateswarlu and Venkata Lakshmi[20] identified that the rate of heat transfer declines with a refinement in the radiation parameter in the proximity of convective boundary condition. Sudarsana Reddy et al.[21] reported the thermal boundary layer thickness is escalates as well as the solutal boundary layer thickness declines with an enhancement in the Brownian motion parameter. Few corresponding articles associated with the sensation of thermal radiation can be found in the Refs. [22–25].

Because of the aforementioned examinations and employments in the direction of liquid movement problems in the proximity of Joule heating, viscous dissipation, thermal radiation, porous medium, and magnetic field, the authors are interested to construct a mathematical pattern of three kinds of nanoliquids with the impact of thermal radiation in the proximity of convective boundary condition along an infinite vertical flat plate.

2. MATHEMATICAL MODEL

We have considered the unsteady natural convection movement and energy transfer of three kinds of nanoliquids past an infinite vertical flat plate. It is supposed that at the initial moment $t = 0$ the nanoliquid is in rest position and is at the fixed ambient temperature T_∞. Suppose that a radiative heat flux vector q_r is associated in the perpendicular direction to the plate. The liquid is a water based nanoliquid including three kinds of nanoparticles: CuO, Ag, and TiO_2, whose thermo physical characteristics are displayed in Table I. The nanopaticles are supposed to have a uniform size and shape. Geometry of the present problem is displayed in Figure 1. All physical quantities are depends on y and t only. In view of these declarations, as well as of the standard Boussinesq's approximation and taking into account the nanoliquid pattern, the dimensional governing equations can be expressed as (See, Refs. [26, 27].

Table I. Thermo-physical characteristics of CuO, Ag, TiO_2 nanoparticles and H_2O.

	CuO	Ag	TiO_2	H_2O
k (W/m K)	76.5	429	8.9538	0.613
ρ (Kg/m^3)	6320	10500	4250	997.1
c_p (J/Kg K)	531.8	235	686.2	4179
$\beta \times 10^{-5}$ (K^{-1})	1.80	1.89	0.9	21

Continuity equation:

$$\frac{\partial v}{\partial y} = 0 \tag{1}$$

Momentum conservation equation:

$$\frac{\partial u}{\partial t} = \frac{\mu_{nf}}{\rho_{nf}} \frac{\partial^2 u}{\partial y^2} + g\beta_{nf}(T - T_\infty) \tag{2}$$

Energy conservation equation:

$$\frac{\partial T}{\partial t} = \frac{k_{nf}}{(\rho c_p)_{nf}} \frac{\partial^2 T}{\partial y^2} - \frac{1}{(\rho c_p)_{nf}} \frac{\partial q_r}{\partial y} \tag{3}$$

The initial and boundary conditions of the momentum and energy equations are given below

$$\left.\begin{aligned} &t = 0: \quad u = 0, \quad T = T_\infty \text{ for all } y \geq 0 \\ &t \geq 0: \quad u = 0, \quad \frac{\partial T}{\partial y} = -\frac{q_w}{k_{nf}} \text{ at } y = 0 \\ &u \to 0, \quad T \to T_\infty \text{ as } y \to \infty \end{aligned}\right\} \tag{4}$$

Here u-liquid motion in x-direction, v-liquid motion in y-direction, t-time, μ_{nf}-dynamic viscosity of nanoliquid, ρ_{nf}-nanoliquid density, g-acceleration due to gravity, β_{nf}-thermal expansion coefficient of nanoliquid, T-liquid temperature, T_∞-stable temperature, k_{nf}-thermal conductivity

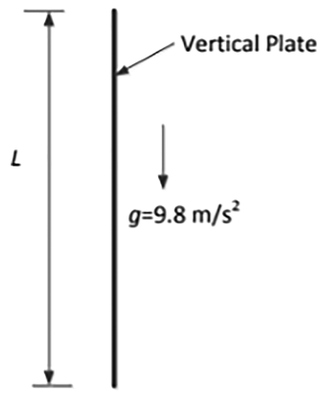

Fig. 1. Sketch of an infinite vertical flat plate.

of nanoliquid, $(c_p)_{nf}$-specific heat of nanoliquid at stable pressure, q_r-radiative flux vector, T_w-temperature of the plate, and q_w-heat flux respectively.

The expressions of μ_{nf}, ρ_{nf}, $(\rho c_p)_{nf}$, and $(\rho\beta)_{nf}$ for spherical nanoparticles can be written as

$$\mu_{nf} = \frac{\mu_f}{(1-\chi)^{2.5}} \tag{5}$$

$$\rho_{nf} = (1-\chi)\rho_f + \chi\rho_s \tag{6}$$

$$(\rho c_p)_{nf} = (1-\chi)(\rho c_p)_f + \chi(\rho c_p)_s \tag{7}$$

$$(\rho\beta)_{nf} = (1-\chi)(\rho\beta)_f + \chi(\rho\beta)_s \tag{8}$$

The existent thermal conductivity of the nanoliquid can be expressed as

$$k_{nf} = k_f \left[\frac{(k_s + 2k_f) - 2\chi(k_f - k_s)}{(k_s + 2k_f) + \chi(k_f - k_s)} \right] \tag{9}$$

Here μ_f-dynamic viscosity of the base liquid, χ-volume fraction of the nanoparticle, ρ_f-density of the base liquid, ρ_s-density of the nanoparticle, $(c_p)_f$-specific heat of the base liquid, $(c_p)_s$-specific heat of the solid, β_f-thermal expansion coefficient of the base liquid, β_s-thermal expansion coefficient of the solid, k_f-thermal conductivity of the base liquid, and k_s-thermal conductivity of the solid respectively.

The radiative flux vector of an optically thick gray liquid can be expressed as (See, Refs. [28, 29])

$$q_r = -\frac{4\sigma^*}{3a^*}\frac{\partial T^4}{\partial y} \tag{10}$$

Here σ^*-Stefan-Boltzmann constant and a^*-mean absorption coefficient respectively.

We suppose that there is a small variation among the liquid temperature T and the stable temperature T_∞, such that T^4 will be expressed as a Taylor's series with respect to T_∞ and omitting the terms of order greater than or equal to two in the series, we acquired

$$T^4 \equiv 4T_\infty^3 T - 3T_\infty^4 \tag{11}$$

Applying the Eqs. (10) and (11) in Eq. (3), we acquired

$$\frac{\partial T}{\partial t} = \frac{k_{nf}}{(\rho c_p)_{nf}}\left[1 + \frac{16\sigma^* T_\infty^3}{3a^* k_{nf}}\right]\frac{\partial^2 T}{\partial y^2} \tag{12}$$

The successive non-dimensional quantities are presented

$$\left.\begin{aligned} U = \frac{u}{\nu_f}L, \quad \tau_1 = \frac{\nu_f}{L^2}t, \quad Y_1 = \frac{y}{L}, \quad \theta = \frac{(T-T_\infty)k_f}{Lq_w}, \\ L = \left[\nu_f^2/g\beta_f T_r\right]^{1/3}, \quad Pr = \frac{k_f}{\nu_f(\rho c_p)_f}, \quad Nr = \frac{16\sigma^* T_\infty^3}{3a^* k_{nf}} \end{aligned}\right\} \tag{13}$$

Equations (2) and (12) converted to the observing non-dimensional pattern

$$\frac{\partial U}{\partial \tau_1} = a_1\frac{\partial^2 U}{\partial Y_1^2} + a_2\theta \tag{14}$$

$$\frac{\partial \theta}{\partial \tau_1} = a_3\frac{\partial^2 \theta}{\partial Y_1^2} \tag{15}$$

In non-dimensional pattern the initial and boundary conditions, can be expressed as

$$\left.\begin{aligned} &\tau_1 = 0: \ U = 0, \quad \theta = 0 \quad \text{for all } Y_1 \geq 0 \\ &\tau_1 > 0: \ U = 0, \quad \partial\theta/\partial Y_1 = -k_f/k_{nf} \quad \text{at } Y_1 = 0 \\ &U \to 0, \quad \theta \to 0 \text{ as } Y_1 \to \infty \end{aligned}\right\} \tag{16}$$

$$\text{Define } Y = Y_1\sqrt{\frac{a_2}{a_1}}, \ \tau = \tau_1 a_2 \tag{17}$$

Applying the Eq. (17) in Eqs. (14) and (15), we acquired

$$\frac{\partial U}{\partial \tau} = \frac{\partial^2 U}{\partial Y^2} + \theta \tag{18}$$

$$\frac{\partial \theta}{\partial \tau} = a_4\frac{\partial^2 \theta}{\partial Y^2} \tag{19}$$

The initial and boundary conditions can be transformed to the pattern

$$\left.\begin{aligned} &\tau = 0: \ U = 0, \ \theta = 0 \text{ for all } Y \geq 0 \\ &\tau > 0: \ U = 0, \ \partial\theta/\partial Y = -\left[k_f/k_{nf}\right]\sqrt{a_1/a_2} \text{ at } Y = 0 \\ &\qquad U \to 0, \quad \theta \to 0 \text{ as } Y \to \infty \end{aligned}\right\} \tag{20}$$

Using the nanoliquid motion and temperature, the shear stress τ_w and heat flux q_w are acquired as

$$\tau_w = \mu_{nf}\left[\frac{\partial u}{\partial y}\right]_{y=0} \tag{21}$$

$$q_w = -k_{nf}\left[\frac{\partial T}{\partial y}\right]_{y=0} \tag{22}$$

In non-dimensional pattern, the skin-friction coefficient Cf and heat transfer coefficient Nu can be expressed as

$$Cf = \frac{\tau_w}{\rho_f(\nu_f/L)^2} \tag{23}$$

$$Nu = \frac{L}{k_f}\frac{q_w}{T_r} \tag{24}$$

On substituting the Eqs. (21) and (22) into Eqs. (23) and (24), we acquired the physical parameters

$$Cf = \sqrt{\frac{a_2}{a_1}}\frac{1}{(1-\chi)^{2.5}}\left[\frac{\partial U}{\partial Y}\right]_{Y=0} \tag{25}$$

$$Nu = -\sqrt{\frac{a_2}{a_1}}\frac{k_{nf}}{k_f}\left[\frac{\partial \theta}{\partial Y}\right]_{Y=0} \tag{26}$$

3. EXACT SOLUTION

Now we solve the Eqs. (18) and (19) subject to the initial and boundary conditions in Eq. (20) by Laplace transform technique.

$$\text{Define } \eta = \frac{Y}{2\sqrt{\tau}},\ U = \tau^{3/2} V(\eta),\ \text{and } \theta = \frac{k_f}{k_{nf}}\sqrt{\tau}\,\phi(\eta) \tag{27}$$

Then Eqs. (18) and (19) are transformed into the pattern

$$\frac{d^2V}{d\eta^2} + 2\eta\frac{dV}{d\eta} - 6V = -4\frac{k_f}{k_{nf}}\phi \tag{28}$$

$$a_4\frac{d^2\phi}{d\eta^2} + 2\eta\frac{d\phi}{d\eta} - 2\phi = 0 \tag{29}$$

The boundary conditions can be written as

$$\left.\begin{array}{ll} V(0) = 0, & \phi'(0) = -4a_{10} \\ V(\infty) = 0, & \phi(\infty) = 0 \end{array}\right\} \tag{30}$$

Exact solution can be acquired by applying the Laplace transform technique stated as follows

$$\overline{V}(p) = \int_0^\infty V(\eta)\,\exp(-p\eta)\,d\eta \tag{31}$$

$$\overline{\phi}(p) = \int_0^\infty \phi(\eta)\,\exp(-p\eta)\,d\eta \tag{32}$$

Exact solutions of Eqs. (28) and (29) are presented in the following form after simplification

$$V(\eta) = \frac{a_{12}\,[2a_7V_1 + \eta V_2]}{3a_5} \tag{33}$$

$$\phi(\eta) = a_{10}\left[a_7\exp\left(-\eta^2/a_4\right) - \eta\,erfc\left(\eta/\sqrt{a_4}\right)\right] \tag{34}$$

$$U(\eta,\ \tau) = \frac{a_{12}\,\tau^{3/2}\,[2a_7V_1 + \eta V_2]}{3a_5} \tag{35}$$

$$\theta(\eta,\tau) = a_{12}\sqrt{\tau}\left[a_7\exp\left(-\eta^2/a_4\right) - \eta\,erfc\left(\eta/\sqrt{a_4}\right)\right] \tag{36}$$

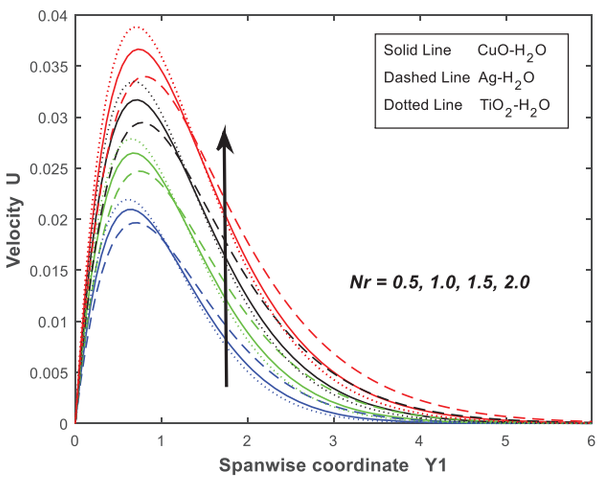

Fig. 2. Interpretation of nanoliquid motion with respect to radiation parameter.

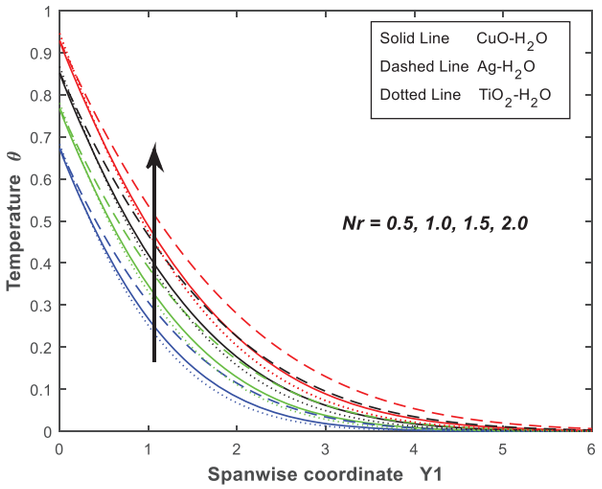

Fig. 3. Interpretation of nanoliquid temperature with respect to radiation parameter.

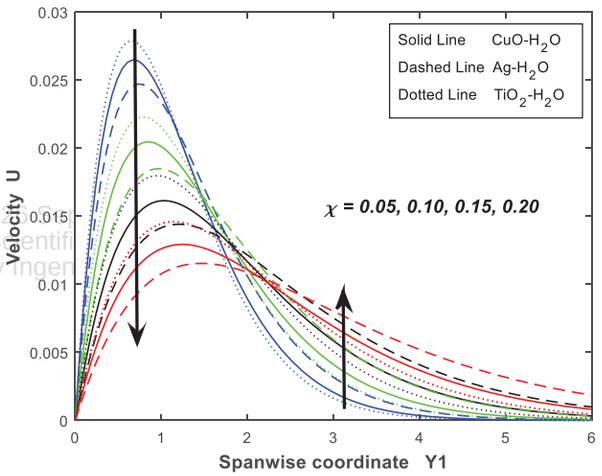

Fig. 4. Interpretation of nanoliquid motion with respect to solid volume fraction.

3.1. Skin Friction Coefficient

Using the nanoliquid motion, the skin friction coefficient can be expressed as

$$Cf = \frac{a_{12}\,a_{13}}{a_{10}}\,\frac{\tau}{(1-\chi)^{2.5}} \tag{37}$$

3.2. Heat Transfer Coefficient

Using the nanoliquid heat transfer, the heat transfer coefficient can be expressed as

$$Nu = \frac{a_{10}\,a_{14}}{a_{12}}\,\frac{1}{\sqrt{\tau}} \tag{38}$$

4. RESULTS AND DISCUSSION

To memorize the consequence of various parameters like thermal radiation parameter Nr, solid volume fraction χ,

ARTICLE

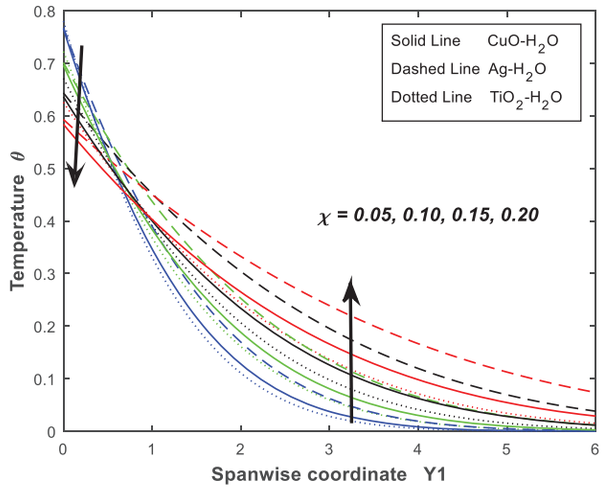

Fig. 5. Interpretation of nanoliquid temperature with respect to solid volume fraction.

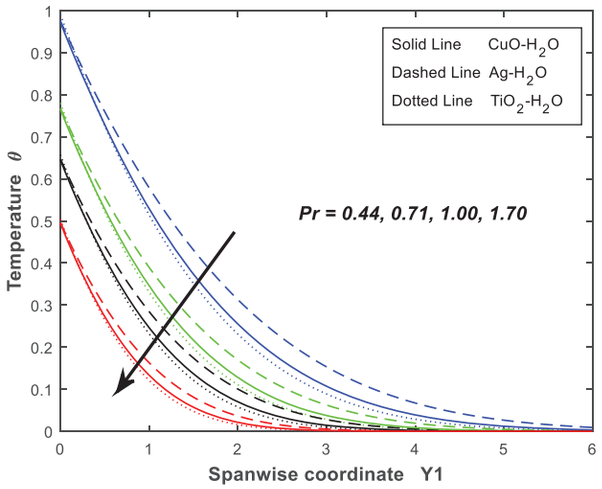

Fig. 7. Interpretation of nanoliquid temperature with respect to Prandtl number.

Prandtl number Pr, and time τ_1 on the flow configuration, the numerical values of the nanoliquid motion U, temperature θ, shear stress Cf, and heat transfer coefficient Nu are computed. In the present study, the following parameter values are utilized for numerical computations: $\chi = 0.05$, $\Pr = 0.71$, $Nr = 1$, and $\tau_1 = 0.2$. In the figures solid line corresponds to copper oxide-water nanoliquid ($CuO–H_2O$) case, dashed line corresponds to silver-water nanoliquid ($Ag–H_2O$) case, and dotted line corresponds to titanium dioxide-water nanoliquid ($TiO_2–H_2O$) case. MATLAB (2015a) program is written to acquire the numerical results of the current work.

The impact of radiation parameter on the nanoliquid motion and heat transfer profiles for three kinds of nanoparticles CuO, Ag, and TiO_2 is demonstrated in Figures 2 and 3. The nanoliquid motion and heat transfer profiles appreciate as radiation parameter propagates.

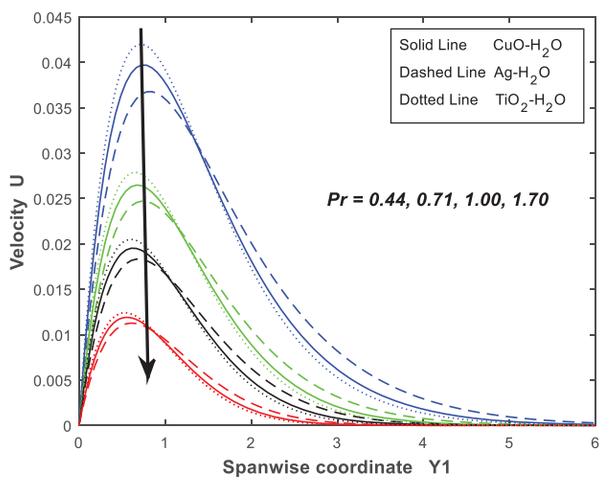

Fig. 6. Interpretation of nanoliquid motion with respect to Prandtl number.

Figures 4 and 5 display the implication of solid volume fraction on the nanoliquid motion and heat transfer profiles for three types of nanoparticles CuO, Ag, and TiO_2. From these graphs, growing solid volume fraction is seen to have a decaying impact on the stream generation in a portion close to the plate as well as contrary trend is identified in a portion away from the plate. So the nanoliquid motion and heat transfer profiles are escalating functions of solid volume fraction in a region away from the plate. Figures 6 and 7 demonstrate the consequence of Prandtl number with respect to the nanoliquid motion and heat transfer profiles for three kinds of nanoparticles CuO, Ag, and TiO_2. The nanoliquid motion and heat transfer declines as Prandtl number propagate. Figures 8 and 9 display the nanoliquid motion and heat transfer for three types of nanoparticles CuO, Ag, and TiO_2 with the progress of time. In Figures 8 and 9 it is identified that, the effectiveness of

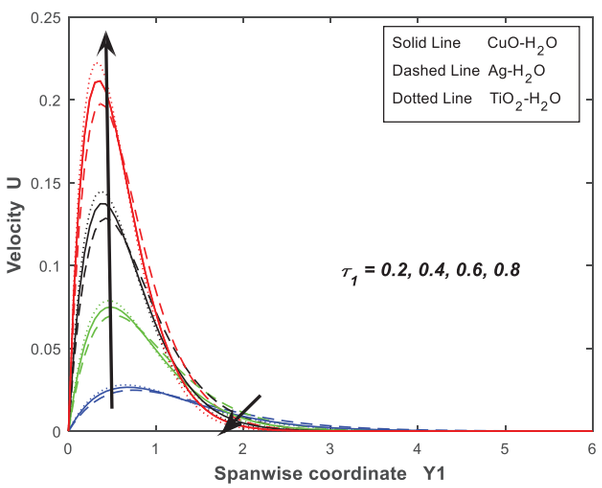

Fig. 8. Interpretation of nanoliquid motion with respect to time.

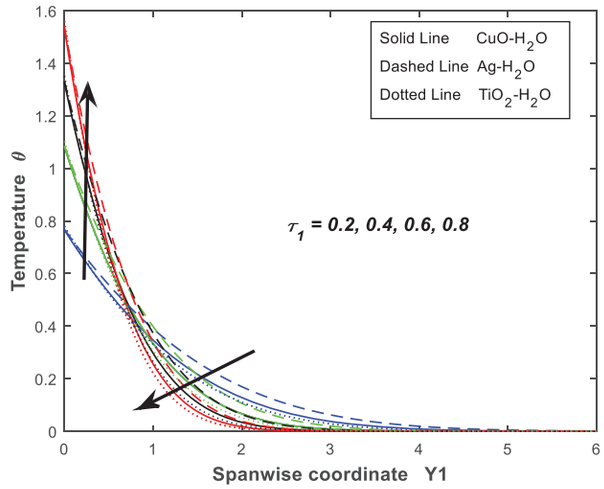

Fig. 9. Interpretation of nanoliquid temperature with respect to time.

the nanoliquid motion and heat transfer is directly proportional to the time in a portion close to the plate as well as nanoliquid motion and heat transfer declines in a portion away from the plate with progress of time.

Visualization the shear stress is of significant application in several engineering designs. Having broad vision into this coefficient will develop designs in storage efficiency, bridges, dams, and drug transmission for cancer sufferer. In Tables II–IX, the numerical values of the shear stress and rate of heat transfer in the proximity of thermal radiation parameter, solid volume fraction, Prandtl number, and time for three kinds of nanoparticles CuO, Ag, and TiO_2 are displayed respectively. It is identified that the shear stress escalates with the accelerating values of radiation parameter and time as well as declines with solid volume fraction and Prandtl number for three kinds of nanoparticles. The rate of heat transfer is extended with escalating values of the solid volume fraction and Prandtl number while rate of heat transfer declined with the accelerating values of radiation parameter and with the progress of time.

Table II. Interpretation of skin friction coefficient with respect to thermal radiation.

Nr	CuO	Ag	TiO_2
0.5	0.1521	0.1489	0.1556
1.0	0.1822	0.1778	0.1872
1.5	0.2095	0.2040	0.2158
2.0	0.2348	0.2283	0.2423

Table III. Interpretation of skin friction coefficient with respect to solid volume fraction.

χ	CuO	Ag	TiO_2
0.05	0.1822	0.1778	0.1872
0.10	0.1612	0.1566	0.1684
0.15	0.1451	0.1417	0.1530
0.20	0.1324	0.1309	0.1401

Table IV. Interpretation of skin friction coefficient with respect to Prandtl number.

Pr	CuO	Ag	TiO_2
0.44	0.2501	0.2431	0.2576
0.71	0.1822	0.1778	0.1872
1.00	0.1441	0.1411	0.1477
1.70	0.0983	0.0968	0.1010

Table V. Interpretation of skin friction coefficient with respect to time.

τ_1	CuO	Ag	TiO_2
0.2	0.1822	0.1778	0.1872
0.4	0.3644	0.3556	0.3743
0.6	0.5466	0.5334	0.5615
0.8	0.7287	0.7112	0.7487

Table VI. Interpretation of heat transfer coefficient with respect to thermal radiation parameter.

Nr	CuO	Ag	TiO_2
0.5	1.4910	1.4856	1.4652
1.0	1.3065	1.3021	1.2816
1.5	1.1770	1.1732	1.1532
2.0	1.0797	1.0763	1.0571

Table VII. Interpretation of heat transfer coefficient with respect to solid volume fraction.

χ	CuO	Ag	TiO_2
0.05	1.3065	1.3021	1.2816
0.10	1.4366	1.4263	1.3844
0.15	1.5717	1.5540	1.4898
0.20	1.7128	1.6861	1.5980

Table VIII. Interpretation of heat transfer coefficient with respect to Prandtl number.

Pr	CuO	Ag	TiO_2
0.44	1.0285	1.0250	1.0089
0.71	1.3065	1.3021	1.2816
1.00	1.5506	1.5453	1.5209
1.70	2.0217	2.0148	1.9831

Table IX. Interpretation of heat transfer coefficient with respect to time.

τ_1	CuO	Ag	TiO_2
0.2	1.3065	1.3021	1.2816
0.4	0.9239	0.9207	0.9062
0.6	0.7543	0.7518	0.7399
0.8	0.6533	0.6510	0.6408

ARTICLE

ARTICLE

5. CONCLUSIONS

The principle conclusions of this article are presented below:

- The order of the nanoliquid motions is Ag $\leq$ CuO $\leq$ TiO_2 in a portion close to the plate and the order is reversed in a portion away from the plate in the proximity of thermal radiation, solid volume fraction, Prandtl number, and time.
- The least heat transfer occurs for TiO_2 nanoliquid and the greatest heat transfer occurs for Ag nanoliquid in the proximity of radiation parameter and Prandtl number.
- The least heat transfer occurs for CuO nanoliquid and the greatest heat transfer occurs for TiO_2 nanoliquid in a portion close to the plate as well as the least heat transfer occurs for TiO_2 nanoliquid and the greatest heat transfer occurs for Ag nanoliquid in a portion away from the plate in the proximity of solid volume fraction.
- The least heat transfer occurs for CuO nanoliquid and the greatest heat transfer occurs for TiO_2 nanoliquid in a portion close to the plate as well as the least heat transfer occurs for TiO_2 nanoliquid and the greatest heat transfer occurs for Ag nanoliquid in a portion away from the plate with the progress of time.
- The order of the skin friction coefficients is Ag < CuO < TiO_2 and hence the least shear stress occurs for Ag nanoliquid as well as the greatest shear stress occurs for TiO_2 nanoliquid.
- The order of the heat transfer coefficients is TiO_2 < Ag < CuO and hence the least heat transfer coefficient occurs for TiO_2 nanoliquid as well as the greatest heat transfer coefficient occurs for CuO nanoliquid.

This article has been confined to three kinds of nanoliquids under the convective boundary condition in the proximity of thermal radiation. Future studies of the present article can be done in distinct directions such as the adjustment of porous medium, Joule heating, Maxwell nanoliquids, micropolar nanoliquids, Casson nanoliquids, thermo-physical properties of nanoliquids, and shape of nanoparticles. In particular, it is proposed that the current work will stimulate experimental studies in high-temperature plasmas, cooling of nuclear reactors, chemical processing equipment, and electronic components to explore supplemental applications in technology.

APPENDIX

$$a_1 = \frac{1}{(1-\chi)^{2.5}} \frac{1}{1-\chi+\chi(\rho_s/\rho_f)},$$

$$a_2 = \frac{1-\chi+\chi[(\rho\beta)_s/(\rho\beta)_f]}{1-\chi+\chi(\rho_s/\rho_f)},$$

$$a_3 = \frac{1}{\Pr}\left[\frac{k_{nf}}{k_f}+Nr\right]\frac{1}{1-\chi+\chi[(\rho c_p)_s/(\rho c_p)_f]},$$

$$a_4 = \frac{a_3}{a_1}, \quad a_5 = a_4 - 1,$$

$$a_6 = \frac{a_4}{\sqrt{\pi}}, \quad a_7 = \sqrt{\frac{a_4}{\pi}},$$

$$a_8 = \frac{2\sqrt{a_2 a_3}}{\sqrt{\pi}(a_1+\sqrt{a_1 a_3})},$$

$$a_9 = \sqrt{\frac{a_2}{\pi a_3}}, \quad a_{10} = 2\sqrt{\frac{a_1}{a_2}},$$

$$a_{11} = \frac{1+a_4}{a_4}, \quad a_{12} = \frac{k_f}{k_{nf}}a_{10},$$

$$a_{13} = \frac{a_3}{a_1+\sqrt{a_1 a_3}}, \quad a_{14} = \frac{1}{2}\sqrt{\frac{\pi a_2}{a_3}}$$

$$V_1(\eta) = \exp(-a_{11}\eta^2)[(a_4+\eta^2)\exp(\eta^2) - a_4(1+\eta^2)\exp(\eta^2/a_4)],$$

$$V_2(\eta) = a_4^{3/2}(2\eta^2+3)\,erfc(\eta) - (2\eta^2+3a_4)\,erfc(\eta/\sqrt{a_4})$$

Nomenclature

u	Liquid motion in x-direction
v	Liquid motion in y-direction
g	Acceleration due to gravity
L	Characteristic of length of plate
t	Dimensional time
T	Liquid temperature
k_f	Thermal conductivity of base liquid
k_s	Thermal conductivity of solid
k_{nf}	Thermal conductivity of nanoliquid
$(c_p)_f$	Specific heat of base liquid at stable pressure
$(c_p)_s$	Specific heat of solid at stable pressure
$(c_p)_{nf}$	Specific heat of nanoliquid at stable pressure
p	Laplace transforms parameter
q_r	Radiating flux vector
q_w	Heat flux
T_w	Temperature of the plate
T_∞	Stable temperature
a^*	Mean absorption coefficient
Nr	Radiation parameter
Pr	Prandtl number
Cf	Skin friction coefficient
Nu	Heat transfer coefficient
U	Non-dimensional motion of nanoliquid

Greek Symbols

ρ_f	Density of base liquid
ρ_s	Density of nanoparticle
ρ_{nf}	Nanoliquid density
μ_{nf}	Dynamic viscosity of nanoliquid
μ_f	Dynamic viscosity of base liquid
χ	Volume fraction of nanoliquid
β_f	Thermal expansion coefficient of base liquid

β_s Thermal expansion coefficient of solid
β_{nf} Thermal expansion coefficient of nanoliquid
τ_w Shear stress
ν Kinematic coefficient of viscosity
σ^* Stefan-Boltzmann constant
θ Non dimensional heat transfer

Author Contributions

The authors assisted uniformly to this article and they have read and authorized the final article.

Conflicts of Interest

The authors declare no conflict of interest.

Acknowledgments: It is pleasure to declare our transparent appreciation to the reviewers for their constructive suggestions and comments for renovation of this article.

References and Notes

1. S. Parvin and A. J. Chamkha, *International Communications in Heat and Mass Transfer* 54, 8 (**2014**).
2. P. K. Kameswaran, B. Vasu, P. V. S. N. Murthy, and R. S. R. Gorla, *International Communications in Heat and Mass Transfer* 77, 78 (**2016**).
3. N. S. Shasikumar, B. J. Gireesha, B. Mahanthesh, B. C. Prasanna Kumara, and A. J. Chamkha, *International Journal of Numerical Methods for Heat and Fluid Flow* 29, 3638 (**2019**).
4. M. Veera Krishna and A. J. Chamkha, *Results in Physics* 15 (**2019**), Article ID: 102652.
5. M. Venkateswarlu, M. Prameela, and O. D. Makinde, *J. Nanofluids* 8, 1506 (**2019**).
6. A. S. Dogonchi, T. Armaghani, A. J. Chamkha, and D. D. Ganji, *Arab. J. Sci. Eng.* 44, 7919 (**2019**).
7. M. Ghalambaz, A. Doostani, E. Izadpanahi, and A. J. Chamka, *J. Therm. Anal. Calorim.* 139, 2321 (**2020**).
8. M. Venkateswarlu and P. Bhaskar, *International Journal of Thermofluid Science and Technology* 7, 1 (**2020**).
9. F. Selimefendigil, H. F. Oztop, and A. J. Chamkha, *International Journal of Numerical Methods for Heat and Fluid Flow* 30, 1755 (**2020**).
10. A. J. Chamkha, M. A. Mansour, A. M. Rashad, K. Hadi, and A. Taher, *J. Thermophys. Heat Transfer* 34, 836 (**2020**).
11. M. Venkateswarlu, D. Venkata Lakshmi, and O. D. Makinde, *Heat Transfer Research* 51, 83 (**2020**).
12. A. S. Begum and A. J. Chamkha, *Heat Transfer* 50, 1 (**2021**).
13. A. Bhattacharyya, R. Sharma, M. K. Mishra, A. J. Chamkha, and E. Mamatha, *J. Nanofluids* 10, 600 (**2021**).
14. A. S. Dogonchi, S. R. Mishra, N. Karimi, A. J. Chamkha, and H. Alhumade, *Journal of the Taiwan Institute of Chemical Engineers* 124, 327 (**2021**).
15. A. Shamadhani Begum and A. J. Chamkha, *Heat Transfer* 50, 1 (**2021**).
16. M. Veera Krishna, N. Ameer Ahamad, and A. J. Chamkha, *J. Nanofluids* 10, 259 (**2021**).
17. A. J. Chamkha, C. Issa, and K. Khanafer, *International Journal of Thermal Sciences* 41, 73 (**2002**).
18. M. Venkateswarlu, O. D. Makinde, and D. V. Lakshmi, *J. Nanofluids* 8, 1010 (**2019**).
19. G. Sreedevi, R. Raghavendra Rao, D. R. V. Prasada Rao, and A. J. Chamkha, *Ain Shams Engineering Journal* 7, 383 (**2016**).
20. M. Venkateswarlu and D. Venkata Lakshmi, *Journal of Naval Architecture and Marine Engineering* 18, 55 (**2021**).
21. P. Sudarsana Reddy, P. Sreedevi, and A. J. Chamkha, *Heat Transfer Asian Research* 46, 815 (**2017**).
22. A. J. Chamkha, S. Ahmed, and A. Aloraier, *International Journal of the Physical Sciences* 5, 1212 (**2010**).
23. A. J. Chamkha, S. Abbasbandy, A. M. Rashad, and K. Vajravelu, *Transport in Porous Media* 91, 261 (**2012**).
24. A. Zaib, M. M. Rashidi, A. J. Chamkha, and A. F. Al-Mudhaf, *International Journal of Fluid Mechanics Research* 44, 513 (**2017**).
25. B. Kumar, G. S. Seth, R. Nandkeolyar, and A. J. Chamkha, *International Journal of Thermal Sciences* 146 (**2019**), Article ID: 106101.
26. G. De Vahl Davis, *International Journal for Numerical Methods for Fluids* 3, 249 (**1983**).
27. R. Iwatsu, J. M. Hyun, and K. Kuwahara, *Int. J. Heat Mass Transfer* 36, 1601 (**1993**).
28. M. Venkateswarlu and O. D. Makinde, *Defect and Diffusion Forum* 384, 31 (**2018**).
29. M. Venkateswarlu, O. D. Makinde, and P. Rami Reddy, *J. Nanofluids* 8, 756 (**2019**).

ARTICLE